Geometric percolation thresholds of interpenetrating plates in three-dimensional space

Y. B. Yi and E. Tawerghi
Department of Mechanical and Materials Engineering, University of Denver, Denver, Colorado 80208, USA
(Received 9 December 2008; revised manuscript received 23 February 2009; published 22 April 2009)

The geometric percolation thresholds for circular, elliptical, square, and triangular plates in the three-dimensional space are determined precisely by Monte Carlo simulations. These geometries represent oblate particles in the limit of zero thickness. The normalized percolation points, which are estimated by extrapolating the data to zero radius, are $\eta_c = 0.961\ 4 \pm 0.000\ 5$, $0.864\ 7 \pm 0.000\ 6$, and $0.729\ 5 \pm 0.000\ 6$ for circles, squares, and equilateral triangles, respectively. These results show that the noncircular shapes and corner angles in the plate geometry tend to increase the interparticle connectivity and therefore reduce the percolation point. For elliptical plates, the percolation threshold is found to decrease moderately, when the aspect ratio ε is between 1 and 1.5, but decrease rapidly for ε greater than 1.5. For the binary dispersion of circular plates with two different radii, η_c is consistently larger than that of equisized plates, with the maximum value located at around $r_1/r_2 = 0.5$.

DOI: 10.1103/PhysRevE.79.041134 PACS number(s): 64.60.ah

I. INTRODUCTION

Percolation is referred to as a phenomenon where at least one domain-spanning pathway exists in a physical system. It is closely related to the transport and mechanical properties of multiphase materials. Regardless of the interfacial contact among different material phases, the measurement of the geometric percolation threshold, i.e., the minimum amount of materials required for percolation, is often one of the fundamental tasks in design and optimization of these materials [1,2]. Mathematically, general percolation processes and phenomena have been studied in the past decades, via the development of exact or approximate solutions in a finite or infinite field [3]. The fact that higher aspect ratio phases percolate at lower volume or area fractions in both two-dimensional (2D) and three-dimensional (3D) systems has been well documented; but the quantitative determination of the geometric effects on noncircular or nonspherical particles were relatively recent, due to the intensive computation demanded in the work.

Among the two primary means of estimating percolation points, namely, the analytical approximation [4,5] and the Monte Carlo simulation [6,7], the latter has proved more computationally effective, especially for 3D systems. Extensive work on circular plates or spheres exists in the literature, including the measurement of the percolation threshold for fully penetrable plates of the same size using the frontier-walk method [8] as well as the determination of the critical threshold and exponents for equisized spheres [9,10]. Percolation problems for disks or spheres of different radii were investigated by a binary mixture of particles [11,12]. It was found that the percolation threshold of such a system is typically very close to that of equisized particles. For example, for a half-and-half mixture of smaller and larger particles, the difference in the percolation threshold is lower than 1% for both spheres and circular plates. Further, the research activities on the percolation of disks and spheres were not only limited to solid material phases but also extended to void phases, namely, "void percolation" [13]. More complex geometries involving additional parameters have also been studied, including solid or hollow fibers and tubes [14]. It was reconfirmed that the percolation threshold is strongly dependent on the particle aspect ratio, implying that much less materials are needed for percolation of fibers or other high aspect ratio particles, thus merit the use of material inclusions of elongated shapes. For elliptical particles, simulation results were obtained from circles to needles and an interpolation formula was developed that was believed superior to all other effective-medium theories [15,16]. For ellipsoids, interests were centered on ellipsoids of revolution in which two parameters are needed to define the geometric shape [17]. The extreme oblate limit of platelike particles to the extreme prolate limit of needlelike particles was studied extensively and their asymptotic solutions were derived from curve fitting. The effect of dimensionality, i.e., the crossover from 2D to 3D ellipsoidal systems, was also investigated computationally [18]. Finally, the continuum percolation for interpenetrating squares and cubes were also studied using the Monte Carlo method, and the corresponding percolation thresholds accurate to three decimal places were reported [19].

Regardless of these important works in the area, results are missing for a special category of the particulate geometry, i.e., 2D plates oriented in the 3D space. It is of particular interest because circular plates are the limiting cases of oblate ellipsoids of revolution when their thickness approaches zero. Compared to their ellipsoid counterparts, plate-shaped particles can percolate at a much lower volume fraction and therefore have potential applications in engineering practice. In addition, elliptical plates in the 3D orientation correspond to a limiting case where the generalized triaxial ellipsoids have a degenerate axis. Discussions on the percolation threshold of triaxial ellipsoids (as opposed to ellipsoids of revolution), particularly in their degenerate scenarios, have never been attempted in the literature. Further, realistic material inclusions can rarely have perfect circular, spherical, or ellipsoidal shapes. Instead they may possess corner angles and facets. How these geometric factors alter the percolation properties remains unknown. It is our intention in the present work to fill in this gap. We target the geometric effects on the percolation thresholds of platelike

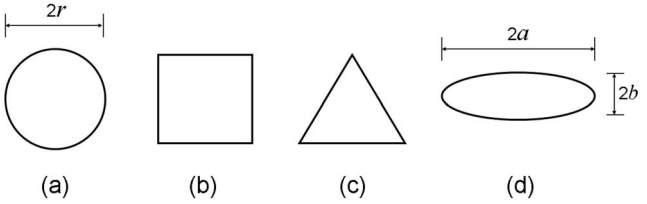

FIG. 1. Four fundamental geometries of plates under investigation.

particles by introducing four fundamental shapes: circles, ellipses, triangles, and squares (as shown in Fig. 1). We first establish the intersection criteria for such geometries and then apply the scaling theories and linear regressions to estimate the percolation thresholds. Comparisons will then be made to infer the effects of geometry on the results.

II. METHODS

A. Percolation detection

A standard computational algorithm for percolation checking has been implemented. In particular, random platelike particles were generated in a unit-cell domain (Fig. 2). The interparticle connectivity as well as the particle-boundary connectivity was checked using the appropriate criteria. The system percolates if there is a connected cluster across the entire domain. The process is intrinsically probabilistic for a finite system and the probability of percolation was determined as simply the ratio of the percolating to the total number of simulations performed. The plate number corresponding to a percolation probability of 50% was recorded as the percolation threshold. This was achieved by a linear interpolation of the percolation probability against the plate number. Results for each condition reported in the current study were generated using at least five separate realizations. Since the probabilistic variation in the results depends on the plate size or the total plate number, an algorithm was developed to make the process more efficient. In particular, the number of realization was variable depending on the plate size. For larger plates, this number was set to a few hundred, whereas for smaller plates, it was set to between five and ten. This treatment was able to greatly reduce the variation in the results, thus increase the solution accuracy.

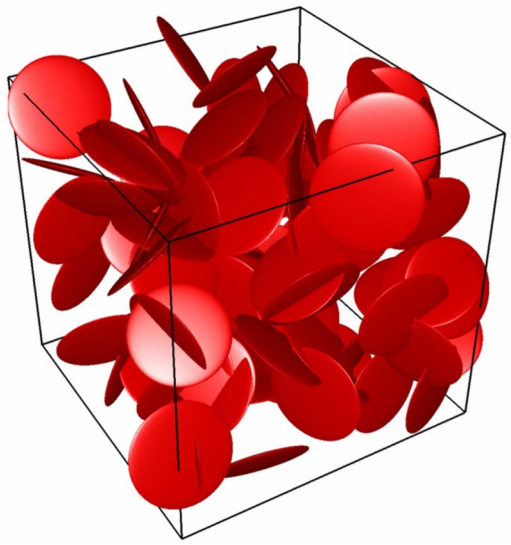

FIG. 2. (Color online) Computer realization of 100 random plates of circular shape in 3D.

The percolation threshold can in principle be expressed in terms of either area fraction for 2D particles or volume fraction for 3D particles. In the current work, where plates are oriented in 3D, because the statistical invariant must be a cubic function of the characteristic length, the definition of *percolation threshold* should be consistent with that of the equivalent 3D systems instead of 2D systems. We define the following variable to measure the percolation threshold:

$$\eta = \frac{4}{3} n \pi r^3, \tag{1}$$

where r is the radius and n is the total plate number. For triangles and squares, r is the equivalent radius of the circular plate having the same area. When r approaches to zero, n will become infinite for percolation, but the value of η will approach an invariant η_c, which is defined here as the "percolation threshold" of the system throughout the paper.

B. Intersection criteria

For circular plates, given two arbitrary plates with radii r_i, normal vectors n_i and center locations (x_i, y_i, z_i) where $i = 1, 2$. Define $\vec{R}$ as the position vector from 1 to 2 and also define the following variables:

$$\cos \alpha = \vec{n}_1 \cdot \vec{n}_2, \tag{2}$$

$$\xi = \vec{R} \cdot \vec{n}_1 / \sin \alpha, \tag{3}$$

$$\vec{n}_c = \vec{n}_1 \times \vec{n}_2, \tag{4}$$

$$x_a = \frac{\vec{R} \cdot \vec{n}_c}{|\vec{n}_c|} + \sqrt{r_2^2 - \xi^2}, \tag{5}$$

$$x_b = \frac{\vec{R} \cdot \vec{n}_c}{|\vec{n}_c|} - \sqrt{r_2^2 - \xi^2}, \tag{6}$$

$$y = \frac{\vec{R} \cdot (\vec{n}_1 \times \vec{n}_c)}{|\vec{n}_1 \times \vec{n}_c|} - \xi(\vec{n}_1 \cdot \vec{n}_2), \tag{7}$$

$$x_p = \sqrt{r_1^2 - y^2}, \tag{8}$$

then in the following two cases, the two circular plates will intersect:

$$\text{Case } 1: r_2^2 - \xi^2 > 0, \quad \{x_a^2 + y^2 \le r_1^2 \text{ or } x_b^2 + y^2 \le r_1^2\}, \tag{9}$$

$$\text{Case } 2: r_2^2 - \xi^2 > 0, \quad |y| < r_1, \tag{10}$$

$$\{(x_a - x_p)(x_b - x_p) < 0 \text{ or } (x_a + x_p)(x_b + x_p) < 0\}.$$

For elliptical plates, there is no closed-form criterion available for checking geometric intersection. The computational strategy here is to take one plate (plate α) as a reference plate and choose the frame of reference such that the major and minor axes of the plate are aligned with x and y axes of the global coordinate system. The circumference of the other plate (plate β) is then divided into a number of small segments in search of the intersection point between the boundary of plate β and the plane formed by plate α.

Case 1: assume there are no intersection points between the line segments and plate α, then the two plates do not intersect. Case 2: assume there are two points of intersection (x_a, y_a) and (x_b, y_b) and

$$y_0 = \frac{y_a x_b - y_b x_a}{x_b - x_a}, \tag{11}$$

$$k = \frac{y_b - y_a}{x_b - x_a}, \tag{12}$$

$$A = \frac{1}{a^2} + \frac{k^2}{b^2}, \quad B = \frac{2y_0 k}{b^2}, \quad C = \frac{y_0^2}{b^2} - 1, \tag{13}$$

$$\Delta = B^2 - 4AC, \tag{14}$$

$$x_p = \frac{-B + \sqrt{\Delta}}{2A}, \quad x_q = \frac{-B - \sqrt{\Delta}}{2A}, \tag{15}$$

where a and b are the half lengths of the major and minor axes of plate α, respectively. Then, in the following case, the two plates intersect:

$$\Delta > 0, \quad \{(x_a - x_p)(x_b - x_p) < 0 \text{ or } (x_a - x_q)(x_b - x_q) < 0\}. \tag{16}$$

In all other situations, the plates do not intersect.

The same strategy is applicable to square and triangular plates—that is, we choose one plate as the reference plate and discretize its boundary into line segments to find the points of intersection between these segments and the plane formed by the other plate. It is then followed by examining the relative positions of these intersection points with respect to the square or triangular surface. However, the total number of the required line segments is greatly reduced here. Only four line segments are needed for a square and three segments for a triangle, as opposed to a least 20 or 30 such segments needed for an ellipse. Hence, the computational efforts can be greatly reduced for squares and triangles compared to elliptical plates.

The above intersection criteria have been validated by graphically realizing the particles in the 3D space followed by an inspection of their physical connectivity. A minimum of 100 random realizations have been examined before they are actually implemented for percolation checking.

For the binary dispersion of disks of different radii, we focus our interest in disks of two different radii r_1 and r_2 where $r_1 < r_2$. Assume the two types of disks have the same number and therefore $f = 0.5$ where f represents the fraction of smaller disks. Define r as the mean radius, i.e., $r = (r_1 + r_2)/2$, and $\lambda = r_1/r_2$, $0 \le \lambda \le 1$, then

$$r_1 = \frac{2\lambda r}{1 + \lambda}, \quad r_2 = \frac{2r}{1 + \lambda}. \tag{17}$$

Further, we fix the total disk number in this binary system while we chose the value of r such that the corresponding η defined in Eq. (1) is maintained the same as that of the equisized disk system. If the equisized disks have radius r_0 then the relationship between r and r_0 is

$$r = \frac{(1 + \lambda) r_0}{\sqrt[3]{4(1 + \lambda^3)}}. \tag{18}$$

Based on these assumptions, simulations can be performed in a procedure similar to equisized disk systems and the resulting percolation thresholds η_c can be evaluated.

C. Error analysis

The numerical error associated with the extrapolated critical percolation point η_c can be estimated in the following method. Assume there is a data array containing n pairs of r and η (r_i, η_i), according to the linear regression theory, we have

$$\eta = a_0 + a_1 r, \tag{19}$$

where

$$a_1 = \frac{n\sum_{i=1}^{n} (r_i \eta_i) - \sum_{i=1}^{n} r_i \sum_{i=1}^{n} \eta_i}{n\sum_{i=1}^{n} r_i^2 - \left(\sum_{i=1}^{n} r_i\right)^2} \tag{20}$$

and

$$a_0 = \frac{\sum_{i=1}^{n} \eta_i \sum_{i=1}^{n} r_i^2 - \sum_{i=1}^{n} r_i \sum_{i=1}^{n} r_i \eta_i}{n\sum_{i=1}^{n} r_i^2 - \left(\sum_{i=1}^{n} r_i\right)^2}. \tag{21}$$

The corresponding confidence intervals for σ_{a0} and σ_{a1} are

$$\sigma_{a0} = \sigma_0 \sqrt{\frac{\sum_{i=1}^{n} r_i^2}{n\sum_{i=1}^{n} r_i^2 - \left(\sum_{i=1}^{n} r_i\right)^2}} \tag{22}$$

and

$$\sigma_{a1} = \sigma_0 \sqrt{\frac{n}{n\sum_{i=1}^{n} r_i^2 - \left(\sum_{i=1}^{n} r_i\right)^2}}, \tag{23}$$

where we assume that all the data points have the same confidence interval, σ_0 and

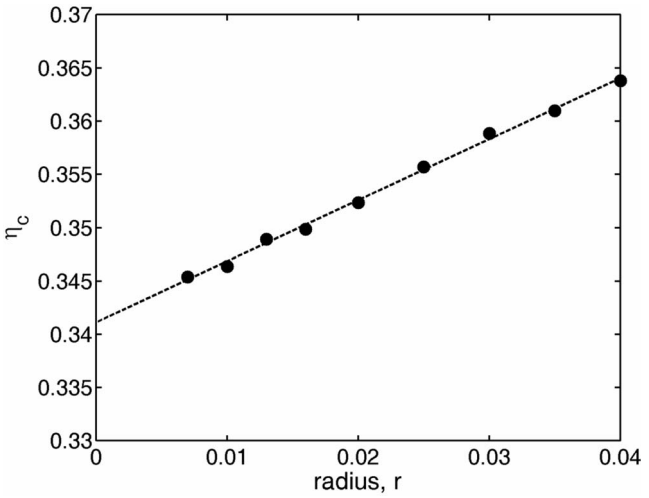

FIG. 3. Determination of percolation threshold for spheres.

$$\sigma_0 = \sqrt{\frac{1}{n}\sum_{i=1}^{n}[y_i - (a_0 + a_1 x_i)]^2}. \quad (24)$$

Clearly, the critical percolation point η_c at $r=0$ is equal to a_0 and the associated standard deviation is equivalent to σ_{a0}.

III. RESULTS

The percolation algorithm was first validated against the equisized spheres system whose solution is well known. The simulation results are presented in Fig. 3. The percolation threshold was computed from nine different radii ranging from 0.007 to 0.04. The total number of particles was from approximately 240 000 to 1300 accordingly. To minimize the numerical error, the simulations were repeated 50 to 1000 times for each particle radius and the computational time was approximately 70 ~ 150 Pentium (D) CPU h for each radius. A linear regression was performed to estimate the percolation threshold corresponding to spheres of zero radius. The extrapolated solution $\eta_c = 0.341\ 2 \pm 0.000\ 3$. This result corresponds to a volume fraction of 28.91%, which is fairly close to the currently most accurate solution 28.9573% obtained by Lorenz and Ziff [10]. This preliminary work can therefore be considered as a validation process for the percolation algorithm developed in the present study.

The same algorithm was subsequently applied to permeable circular plates in the 3D space and the results are shown in Fig. 4. These results were computed from eight different radii ranging from 0.01 to 0.04, with the total number of particles ranging between 230 000 and 3800 accordingly. The extrapolated solution is $\eta_c = 0.961\ 4 \pm 0.000\ 5$. It should be pointed out that this result is noticeably lower than that reported by Garboczi *et al.* [17]. They studied the oblate and prolate ellipsoids and provided an asymptotic solution for oblate particles of zero aspect ratio (that is, zero dimension through the thickness), which should be identical to the solution for circular plates. However, their prediction was $1.27a/b$ in terms of the volume fraction of particles where b is the radius of revolution and a is the semiaxis length. Applying

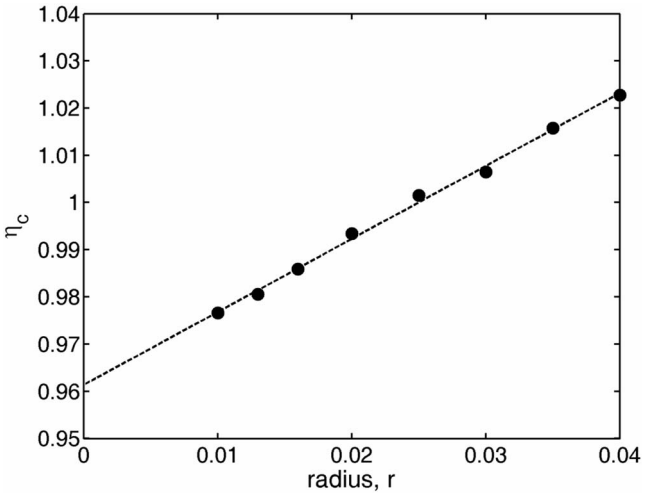

FIG. 4. Determination of percolation threshold for circular plates in 3D.

$$f = 1 - e^{-nV} \approx nV = \frac{4}{3}n\pi ab^2, \quad \text{when} \quad a \to 0, \quad (25)$$

where f represents the volume fraction, V is the volume of each individual particle, and n is the particle number, we have immediately

$$\eta_c = \frac{4}{3}n\pi b^3 \to 1.27, \quad (26)$$

which is apparently much higher than the result predicted in the current study (0.9614). The reason behind this discrepancy is yet unknown. It was noticed in the past that Garboczi's solutions for the percolation thresholds of overlapping ellipsoids were consistently higher than those predicted by other methods [20], and therefore it is not surprising to see the discrepancy in the comparison here.

For square-shaped plates in the 3D space, the results are shown in Fig. 5. The maximum number of plates involved is

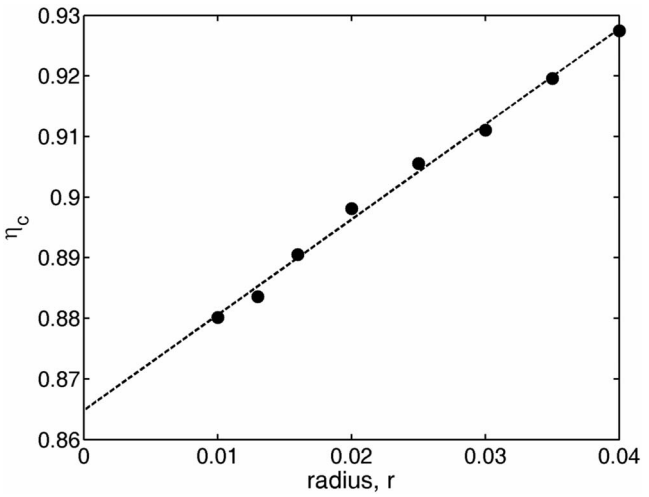

FIG. 5. Determination of percolation threshold for square plates in 3D (r is the equivalent radius of squares).

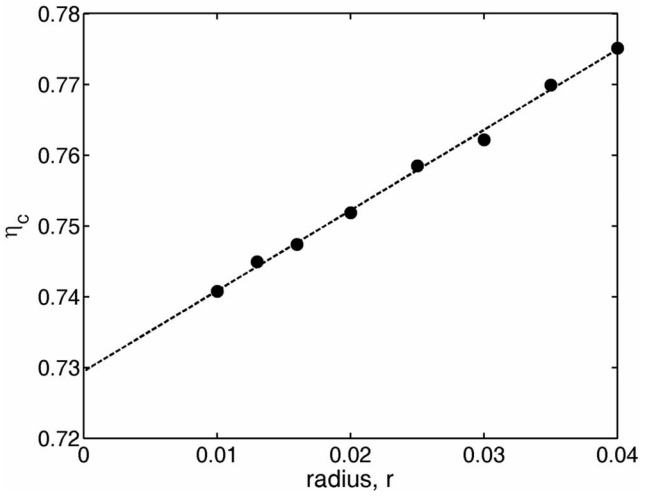

FIG. 6. Determination of percolation threshold for triangular plates in 3D (r is the equivalent radius of triangles).

150 000. The extrapolated percolation threshold at zero size of squares is $\eta_c=0.864\ 7\pm0.000\ 6$. Clearly, this value is lower than that for circular plates, indicating that fewer particles are needed for percolation. This is because the corner angles of squares make it easier for the plates to touch each other, therefore reduce the percolation point. This is consistent with the corner effects elucidated in Baker *et al.*'s [19] work regarding the continuum percolation of 2D squares and 3D cubes.

The results for quadrilateral triangles are shown in Fig. 6. The maximum number of plates is around 430 000, and the predicted percolation threshold is $\eta_c=0.729\ 5\pm0.000\ 6$. Compared to the square-shaped plates, the triangles have slightly more elongated shape at the corners (60° angles in triangles as opposed to 90° angles in squares) therefore facilitate the interparticle connectivity. As a result, the percolation threshold is further reduced. The above results including the mean values and standard deviations for various geometries are tabulated in Table I.

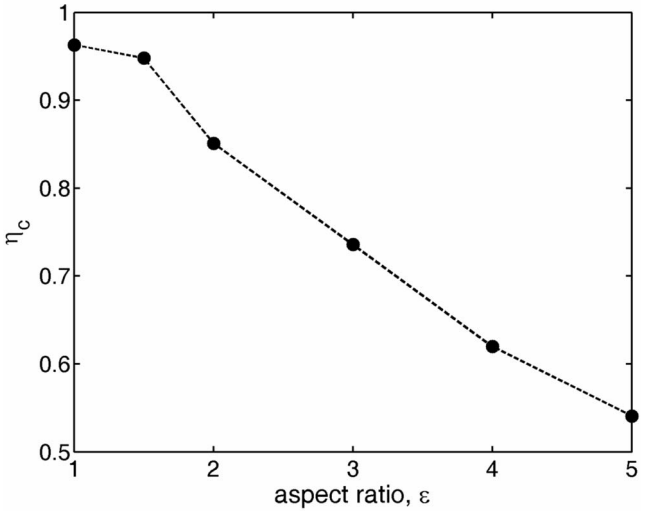

FIG. 7. Percolation threshold as a function of the aspect ratio of elliptical plates in 3D.

TABLE I. Estimates of the percolation thresholds for different geometries in 3D.

	Spheres	Circular plates	Square plates	Triangular plates
η_c	0.3412	0.9614	0.8647	0.7295
Error	±0.0003	±0.0005	±0.0006	±0.0006

The investigation on elliptical plates revealed that the percolation threshold monotonically decreases with the plate aspect ratio (Fig. 7). At $\varepsilon=5$, η_c is only half the value at $\varepsilon=1$, meaning that much fewer particles are needed to reach percolation at higher aspect ratios. This is consistent with both the analytical and computational results reported in the literature. In addition, the results show that the reduction in the percolation threshold is not significant when the aspect ratio is below 1.5 but experiences relatively sharp decrease beyond that point. This agrees with the predicted trends from other elongated particles such as ellipsoids reported in the literature [17]. A maximum of 30 000 particles were realized in the simulations. Each aspect ratio was run for three different radii 0.02, 0.03, and 0.04 for linear extrapolation. Particles with aspect ratio greater than 5 were not studied due to the extremely intensive computation. However, it is expected that the percolation threshold will follow the same monotonic relationship with the aspect ratio beyond that point.

For the binary dispersion of circular plates, f was maintained to be 0.5 and λ was varied from 0.1 to 0.9 with an increment of 0.1 in the simulations. Notice that both $\lambda=0$ and $\lambda=1$ correspond to disks of the same size. Four different mean radii were examined to extrapolate the percolation threshold for each value of λ. The estimated percolation thresholds along with errors are listed in Table II. Clearly, η_c increases at the beginning, reaches a peak value $\eta_c\approx0.981\ 5$ around $\lambda=0.5$, and then decreases. At the two ends where λ is close to 0 or 1, η_c is approaching 0.9616. It is seen that for the entire range of λ, the deviation of η_c from the equisized disk solution is noticeably small not more than 2%. A close inspection also shows the existence of the asymmetry in the result with respect to the midpoint $\lambda=0.5$. These results are consistent with Quintanilla and Ziff's [21] work on the binary dispersion of disks on a 2D plane, although a different peak value location ($\lambda=0.4$ when $f=0.5$) was reported for 2D disks.

IV. CONCLUSIONS

The geometric percolation involving plates in the 3D space has been studied using a Monte Carlo simulation method. Four different geometries are studied: circles, ellipses, squares, and triangles, which represent the geometric limits of oblate particles when one of the axes degenerates to zero. The plate-plate intersection criteria for the four geometries are established analytically. The percolation probability at various equivalent radii is computed and the percolation threshold is estimated at the limit of zero radius by linear extrapolation. An error analysis is successfully applied to estimate the solution tolerance. Comparisons among dif-

TABLE II. Estimates of the percolation thresholds for binary dispersion of circular plates in 3D.

λ	0.1	0.2	0.3	0.4	0.5	0.6	0.7	0.8	0.9
η_c	0.9612	0.9688	0.9734	0.9756	0.9815	0.9788	0.9703	0.9640	0.9616
Error	$\pm$0.0007	$\pm$0.0005	$\pm$0.0007	$\pm$0.0006	$\pm$0.0005	$\pm$0.0007	$\pm$0.0004	$\pm$0.0006	$\pm$0.0006

ferent geometries show that the global or local curvatures tend to increase the interparticle connectivity and thus reduce the percolation point. For elliptical plates, the percolation threshold has been found as a monotonic function of the particle aspect ratio, which is consistent with the results for ellipsoids or planar ellipses. When disks of two different radii are mixed together, the percolation threshold does not change much, with a peak value located where the ratio of the two radii is approximately 0.5. Some results have also been compared to the data reported in the literature. The results and methods used in the current study are useful in predicting conduction and percolation characteristics of multiphase material systems containing oblate particles of thin thickness.

[1] S. Mohanty and M. Sharma, Phys. Lett. A **154**, 475 (1991).
[2] Y. B. Yi, Acta Mater. **56**, 2810 (2008).
[3] S. Torquato, *Random Heterogeneous Materials* (Springer-Verlag, New York, 2002).
[4] A. Coniglio, U. Deangelis, A. Forlani, and G. Lauro, J. Phys. A **10**, 219 (1977).
[5] J. Quintanilla and S. Torquato, Phys. Rev. E **54**, 5331 (1996).
[6] G. E. Pike and C. H. Seager, Phys. Rev. B **10**, 1421 (1974).
[7] D. Dhar, Phys. Rev. Lett. **64**, 1613 (1990).
[8] J. Quintanilla, S. Torquato, and R. M. Ziff, J. Phys. A **33**, L399 (2000).
[9] M. D. Rintoul and S. Torquato, J. Phys. A **30**, L585 (1997).
[10] C. D. Lorenz and R. M. Ziff, J. Chem. Phys. **114**, 3659 (2001).
[11] J. Quintanilla, Phys. Rev. E **63**, 061108 (2001).
[12] R. Consiglio, D. R. Baker, G. Paul, and H. E. Stanley, Physica A **319**, 49 (2003).
[13] Y. B. Yi, Phys. Rev. E **74**, 031112 (2006).
[14] L. Berhan, Y. B. Yi, A. M. Sastry, E. Munoz, M. Selvidge, and R. Baughman, J. Appl. Phys. **95**, 4335 (2004).
[15] W. Xia and M. F. Thorpe, Phys. Rev. A **38**, 2650 (1988).
[16] Y. B. Yi and A. M. Sastry, Phys. Rev. E **66**, 066130 (2002).
[17] E. J. Garboczi, K. A. Snyder, J. F. Douglas, and M. F. Thorpe, Phys. Rev. E **52**, 819 (1995).
[18] Y. B. Yi, C. W. Wang, and A. M. Sastry, J. Electrochem. Soc. **151**, A1292 (2004).
[19] D. R. Baker, G. Paul, S. Sreenivasan, and H. E. Stanley, Phys. Rev. E **66**, 046136 (2002).
[20] Y. B. Yi and A. M. Sastry, Proc. R. Soc. London, Ser. A **460**, 2353 (2004).
[21] J. A. Quintanilla and R. M. Ziff, Phys. Rev. E **76**, 051115 (2007).